Vol. 78 No. 5 ACTA GEOLOGICA SINICA Oct. 2004 1109–1121

Geochemical Records of Mantle Processes in Mantle Xenoliths from Three Cenozoic Basaltic Volcanoes in Eastern China

LIU Congqiang[1], HUANG Zhilong[1], XIE Guanghong[2] and MASUSDA Akimasa[3]
1 *Institute of Geochemistry, Chinese Academy of Sciences, Guiyang, Guizhou 550002 China; E-mail: liucong-qiang@163.net*
2 *Guangzhou Institute of Geochemistry, Chinese Academy of Sciences, Wushan, Guangzhou, Guangdong 510640, China*
3 *Department of Chemistry, Faculty of Science, The University of Tokyo, Hongo, Tokyo 113, Japan*

Abstract Rare earth element (REE) contents, and Sr and Nd isotopic compositions were measured for three suites of mantle xenoliths from the Kuandian, Hannuoba and Huinan volcanoes in the north of the Sino-Korean Platform. From the correlations of Yb contents with Al/Si and Ca/Si ratios, the peridotites are considered to be the residues of partial melting of the primitive mantle. The chondrite-normalized REE compositions are diverse, varying from strongly LREE-depleted to LREE-enriched, with various types of REE patterns. Metasomatic alteration by small-volume silicate melts, of mantle peridotites previously variably depleted due to fractional melting in the spinel peridotite field, can account for the diversity of REE patterns. The Sr/Ba versus La/Ba correlation indicates that the metasomatic agent was enriched in Ba over Sr and La, suggestive of its volatile-rich signature and an origin by fluid-triggered melting in an ancient subduction zone. The Sr and Nd isotopic compositions of these xenoliths, even from a single locality, vary widely, covering those of Cenozoic basalts in eastern China. The depleted end of the Sr-Nd isotope correlation is characterized by clearly higher $^{143}Nd/^{144}Nd$ and a broader range of $^{87}Sr/^{86}Sr$ compared to MORB. The low-$^{143}Nd/^{144}Nd$ and high-$^{87}Sr/^{86}Sr$ data distribution at the other end of data array suggests the existence of two enriched mantle components, like EM1 and EM2. The correlations between $^{143}Nd/^{144}Nd$ and $^{147}Sm/^{N4}Nd$ ratios in these xenoliths suggest at least two mantle metasomatic events, i.e. events at 0.6–1.0 Ga and 280–400 Ma ago.

Key words: mantle xenolith, geochemistry, mantle process, northeastern China

1 Introduction

The geochemical evidence obtained from the studies of the Cenozoic basalts in eastern China has provided the basis for the establishment of the geochemical heterogeneity and identified two isotopically distinct enriched mantle components, the EM1 and EM2 within the subcontinental mantle (e.g. Tu et al., 1989; Song et al., 1990; Basu et al., 1991; Tatsumoto and Nakamura, 1991; Liu et al., 1994). The geochemistry of the mantle xenoliths from several basaltic volcanoes in eastern China has also revealed the existence of these two mantle enriched components in the lithospheric mantle (Song and Frey, 1989; Tatsumoto et al., 1992). Moreover, Tatsumoto et al., (1992) pointed out that the EM1 signals are shown mainly by the host basalts and the EM2 signals by the mantle xenoliths. Hence they argued that the EM2 domain is located in the lithosphere just above the EM1 domain of the basalt source at the lower level of the lithospheric mantle. Recent studies of mantle xenoliths from eastern China focus not only on the geochemical heterogeneities, but also on the mantle processes responsible for the variations in geochemical composition of the mantle (e.g. Ho et al., 2000; Zheng, 1998; Zhang et al., 2000; Zheng et al., 2001; Xu et al., 2003). Although these studies have identified the existence of the distinct mantle components, the mantle processes responsible for their formation are still not well understood.

Trace element geochemistry of mantle xenoliths has often been found decoupled from isotope geochemistry, which is strongly suggestive of a complex chemical evolution history of the mantle. Therefore, trace element studies, especially, of the REEs, when combined with isotopic studies, have been proven powerful not only in identifying different mantle components, but also in investigating the mantle processes that created the geochemical heterogeneity in the mantle. In this paper we present both trace element data mainly of rare-earth elements (REEs) and Sr and Nd isotope data for nineteen mantle xenoliths from three basaltic volcanoes in North China. The main objective of this study is to investigate the processes involved in the evolution of the lithospheric mantle beneath eastern China.

2 Samples

Two major Precambrian domains are recognized in

eastern China, the Sino-Korean and Yangtze Cratons, which are surrounded by younger orogenic belts (Fig. 1). Nuclei of Archaean age are firmly established for the Sino-Korean Craton only. They are composed mainly of high-grade granulitic terrains and greenstone belts (Yang et al., 1986). Conventionally, these crustal nuclei are considered to be the consolidated and aggregated parts of the Archaean salic crust, and the main formation stage of the Sino-Korean Platform is inferred to have started 2.5 Ga ago and to have ended before 1.85 Ga (Yang et al., 1986; Zhang et al., 1986). The mantle-derived xenoliths investigated in this study were collected from three Cenozoic basaltic volcanoes, Hannuoba in Hebei Province, Kuandian in Liaoning Province and Huinan in Jiling Province, all located in the north of the Sino-Korean platform (Fig. 1). From these three volcanoes were sampled large volumes and many types of mantle xenoliths, mainly lherzolites, harzburgites, dunites and pyroxenites. Hydrous xenoliths containing amphibole, phlogopite and mica are also present in small quantities in these volcanoes. Detailed studies on the geological settings, petrology and mineralogy of the host basalts and xenoliths of these three volcanic fields have been reported by several authors (e.g. Cong and Zhang, 1983; Lu et al., 1983; Luo, 1984).

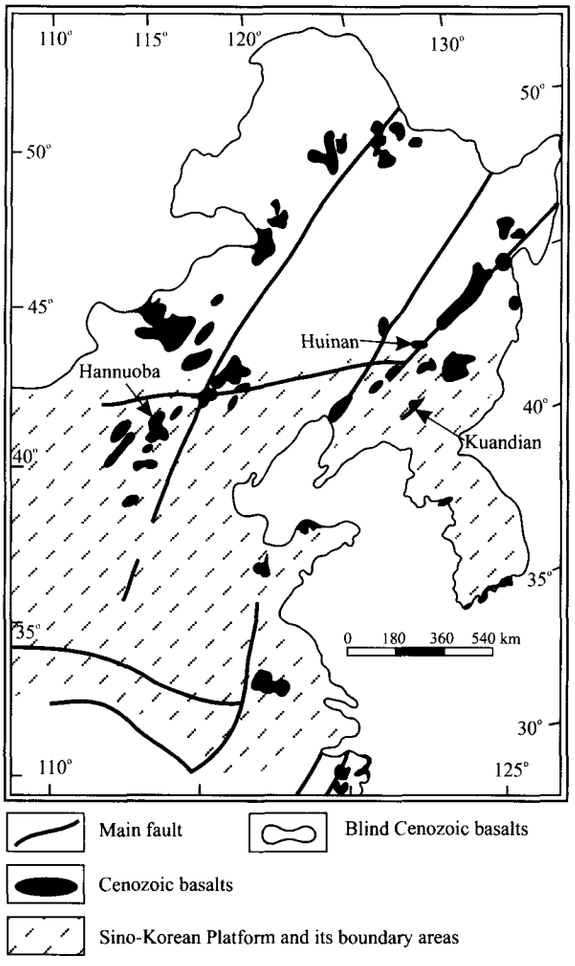

Fig. 1. Map showing the distribution of Cenozoic basalts in north China and the sample locations.

The studied samples range in size from 20 to 30 cm across. The modal mineral compositions of these xenoliths are summarized in Table 1. They were estimated mainly from mineral grain counting after crushing the whole rocks into 0.4 mm size. This procedure was chosen over point-counting of thin sections because the mineral sizes are too large to obtain reliable results by point counting, and it is relatively easy to distinguish the minerals by color in the xenoliths. According to their mineralogical compositions, most of the xenoliths studied here are lherzolites.

Lherzolite and harzburgite xenoliths consist of a mosaic of subhedral to anhedral olivine, orthopyroxene and green clinopyroxene, with minor spinel; grains are generally 1 to 5 mm in size. One lherzolite sample (C-A) contains about 3% amphibole; amphibole and clinopyroxene minerals were separated from this sample for isotope analysis. Deformation textures, such as undulose extinction and weak foliation in olivine or pyroxene, are visible in both host lherzolite and clinopyroxene-rich veins. Two lherzolite xenoliths (H-l and X11) veined by pyroxenite were selected to study the geochemical relationship between the pyroxenite vein and the host lherzolite. The clinopyroxenite veins in lherzolites are generally 15 to 40 mm wide and contain olivine and minor spinel. The composite xenolith H-l contains two veins (H-la and H-lb), which are both about 3 cm thick and 10 cm apart from each other. The wall-rock sample H-l was cut from the portion 2 to 6 cm apart from the border of the vein a (H-1a). The wall-rock sample X-ll was the section 2 to 5 cm apart from the vein-host contact.

The pyroxenite xenoliths studied here can be further divided into garnet pyroxenite and spinel or olivine pyroxenite. The clinopyroxene and orthopyroxene show a polygonal mosaic of grains, suggestive of textural equilibrium. Some large pyroxene grains show undulatory extinction, while other grains show lamellar structures. One pyroxenite contains garnet, and seems to be altered by melts or fluids, because dark brown material was found between minerals under the microscope. Although fluid inclusion trails are present in lherzolite minerals, such inclusions are bigger and more abundant in pyroxenite and clinopyroxene-rich veins.

3 Experimental Procedures

The major element compositions of the xenoliths were determined by X-ray fluorescence method. Whole rocks

and minerals were analyzed for both trace element and isotopic compositions. For whole-rock analyses, the central fresh part of the xenoliths was used in order to avoid possible contamination by host magmas. The minerals, most of which were clinopyroxenes, were separated by hand-picking from the whole rocks after being crushed into pieces of ~0.4 mm diameter. Prior to chemical decomposition, the minerals were ultrasonically washed with distilled water, then with 2M HCl, followed by dilute HF (5%) and finally by distilled water.

The trace element abundances were measured by the single spike isotope dilution method on a JEOL JMS-05RB mass spectrometer in the Department of Chemistry, The University of Tokyo. Chemical blanks are negligibly small for the analyzed trace elements. The absolute uncertainties involved in the isotope dilution analyses were 0.5%–2% for all of the analyzed elements. Sr and Nd isotopic compositions were determined on a VG354 mass spectrometer equipped with five Faraday collectors. The isotope ratios were normalized to $^{87}Sr/^{86}Sr$=0.1194 for Sr and to $^{143}Nd/^{144}Nd$= 0.7219 for Nd. The average $^{143}Nd/^{144}Nd$ for the La Jolla Nd standard was 0.511846±0.000016 (n=10) and $^{87}Sr/^{86}Sr$ for the NBS987 Sr standard was 0.710245±0.000022 (n=12) during the measurement period of these samples.

4 Results

4.1 Major and trace elements

Table 2 lists the major element compositions of the samples. The peridotite samples have MgO contents ranging from 34% to 43.8%, but their Mg numbers are relatively constant ($Mg^{\#}$=87–92). The Al_2O_3 and CaO contents vary from 0.89% to 3.92% and from 0.5% to 3.55%, respectively. The distributions of Mg/Si, and Ca/Si vs. Al/Si of these samples, together with those of the spinel and garnet peridotites from eastern China, follow a general geochemical fractionation trend, with the more refractory samples (basalt depleted) plotting closer to olivine-rich end member. Two samples (H-1 and J118C7) have the Mg/Si ratios lower than the estimated primitive mantle, although their Al/Si ratios (and also their Sr and Nd isotopic ratios) do not suggest that they are primitive. The pyroxenite xenoliths and veins are distinguished from the peridotites by their low Mg/Si ratios. The Al/Si and Ca/Si ratios for them are variable, which shows control by the mineral assemblage of clinopyroxene, garnet and orthopyroxene.

The trace element abundances are listed in Table 3, and the chondrite-normalized REE patterns shown in Fig. 2. Since clinopyroxene is the main REE and Sr bearing mineral (Stosch and Lugmair, 1986; Stosch et al., 1986; Song and Frey, 1989), the clinopyroxene separates, rather than the whole rocks, were measured for most samples. For two samples, the trace element abundances of both clinopyroxene separates and bulk rocks were analyzed. The REE patterns of the clinopyroxene separate and bulk rock of sample A-21 have almost the same shape, suggesting the dominance of clinopyroxene as REE-containing mineral phase (Fig. 2a). In contrast, clinopyroxene separated from garnet pyroxenite (J112C3) has a clearly different REE pattern from the whole rock. The clinopyroxene has a convex-upward REE pattern, while the REE pattern of the bulk rock is flat from Sm to Lu with an upward pattern from Sm to La. This discrepancy between the clinopyroxene and the bulk rock indicates the importance of garnet as the HREE-containing phase as well as the existence of LREE-enriched phases.

Table 1 Mineral modes (volume %) of mantle xenoliths from northern China

Sample	Olivine	Opx	Cpx	Spinel	Garnet	Amph	Rock type
Kuandian							
C-A	58	21	17	1		3	Lherzolite
J118C7	55	26	18.6	0.4			Lherzolite
J20C18	60	22	17	1			Lherzolite
J36C3	64	18.1	17	0.9			Lherzolite
J50C3	72	15	12	1			Lherzolite
J112C3	10	38.4	43.9	0.4	7.1		Websterote
Huinan							
A-15	65	22	12.3	0.7			Lherzolite
A-18	60	26	13	1			Lherzolite
A-20	70	22	7.2	0.8			Harzburgite
A-21	29	29	41	1			Websterite
A-25	65	24	10.1	0.9			Lherzolite
A-26	66	24.5	8.5	1			Lherzolite
A-27	57	23	19.1	0.9			Lherzolite
Hannuoba							
H-1	56	27	16	1			Lherzolite
H-1a (vein ain H-1)	6.5	43	48.5	2			Websterite
H-1b (vein b in H-1)	23.5	20	56	0.5			Websterite
H-2		61	37	1			Websterite
H-3	68	24	7	1			Harzburgite
H-4	50	28	20	2			Lherzolite
X-11	55	26	18.2	0.8			Lherzolite
X-11a (vein in X-11)	20	25	54	1			Websterite
X-14	55	30	14	1			Lherzolite

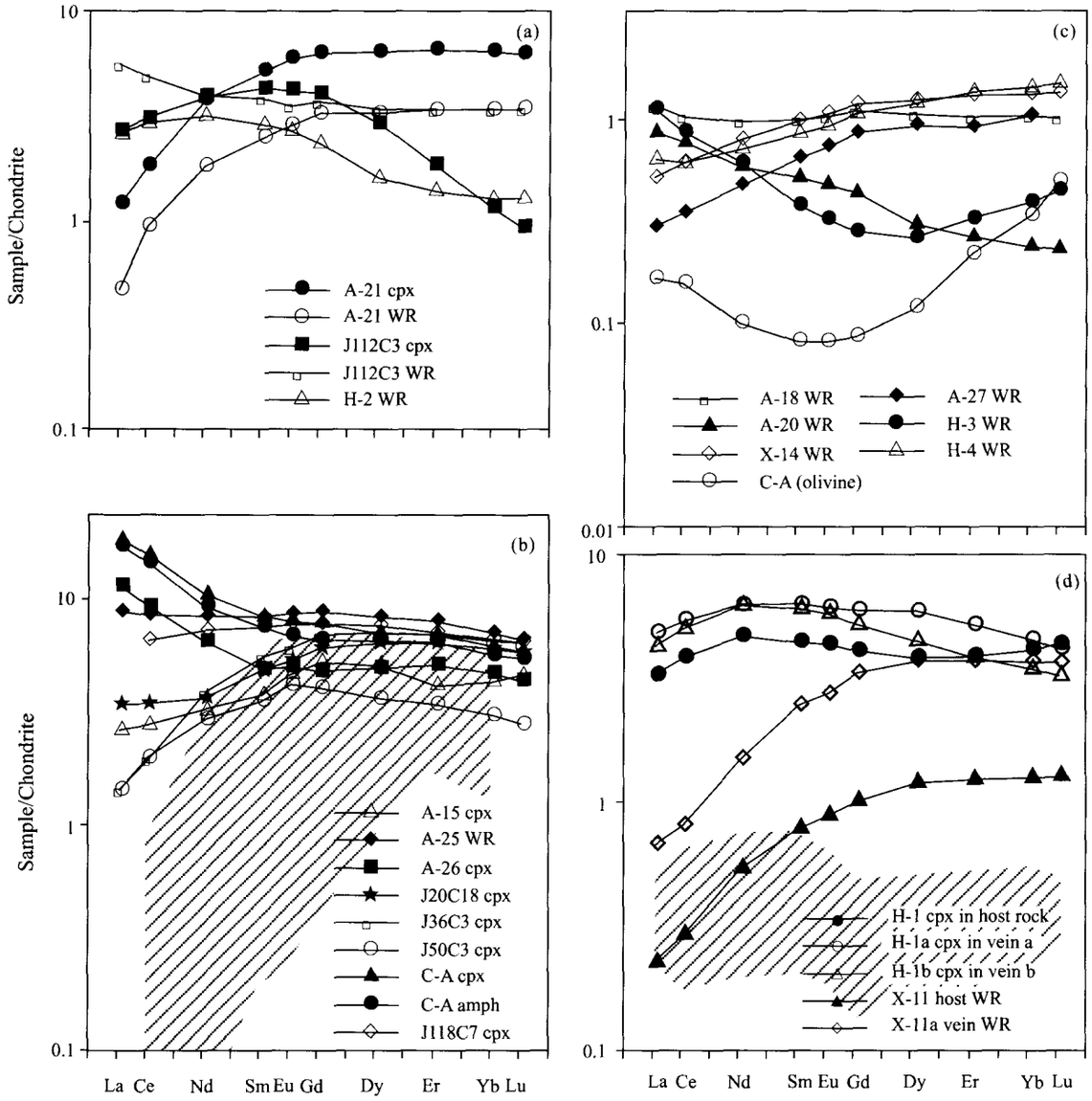

Fig. 2. Chondrite (Leedey)-normalized REE abundances of the mantle xenoliths.
The hatchures area in diagram b is the distribution of clinopyroxene separates from abyssal peridotites studied by Johnson et al. (1990), and in diagram d is that of host harzburgite at < 15 cm from the vein-host contact (Bodinier et al., 1990).

Analyses of both minerals and bulk rocks show diverse REE compositions. The REE patterns of the clinopyroxene separates and the bulk rocks both vary from LREE-enriched to LREE-depleted types (Fig. 2b & 2c). Moreover, the absolute HREE contents are also highly variable. As compared to the clinopyroxene separates from abyssal peridotites, the clinopyroxenes studied here are more LREE-enriched and generally have higher HREE contents. Concave LREE, or spoon-shaped REE patterns were found in two lherzolite samples. One harzburgite and an olivine sample have U-shaped REE patterns, with depletions of the middle REEs. Among the bulk rocks, the harzburgites have the lowest heavy REE contents.

The clinopyroxenes from pyroxenite xenoliths or veins show two types of REE patterns, LREE-depleted and convex-upward REE patterns (Fig. 2a & 2d). The former was found in samples A-21 and X-11; the latter was found in samples J112C3, H-1a and H-1b. The convex-upward REE patterns are very similar to those of clinopyroxene megacrysts formed at depth in equilibrium with basaltic magmas from Kuandian and Hannuoba (Liu et al., 1992a). The clinopyroxene separates and the bulk rock of the

pyroxenite xenolith A-21, and the bulk-rock pyroxenite vein and the host lherzolite of sample X-11 have identical LREE-depleted patterns. In summary, the pyroxenite xenoliths or veins that contain higher olivine and orthopyroxene have LREE-depleted patterns, while those with dominant clinopyroxene have the convex-upward REE patterns.

Although the pyroxenes separated respectively from the pyroxenite veins (H-1a and H-1b) have similar convex-upward REE patterns, the pyroxenes from the vein H-1a have relatively higher HREE and La and Ce contents. The clinopyroxenes from the host lherzolite (H-l) have a similar convex-upward REE patterns from La to Dy to the vein pyroxenite, but show an increase from Dy to Lu.

4.2 Sr and Nd isotopic compositions

The Sr and Nd isotope ratios measured for these xenoliths vary from 0.702437 to 0.705749 and 0.512619 to 0.513321 (Table 3 and Fig. 3), respectively. The highest Nd isotope ratio found by Song and Frey (1989) in the Hannuoba peridotite xenoliths is 0.5135. The Nd isotope ratio of $^{143}Nd/^{144}Nd=0.5113$ found by Tatsumoto et al. (1992) in the Hannuoba phlogopite pyroxenite, and a ratio of $^{143}Nd/^{144}Nd=0.511865$ in this work in a pyroxenite sample, which are not plotted in Fig. 4, form the other extreme of the data array. The large variation in isotopic composition of the mantle xenoliths strongly demonstrates the geochemical heterogeneity of the mantle sampled as these xenoliths. The array end with high Sr and low Nd isotope ratios tends to stretch out respectively towards EM1 and/or EM2. Comparatively, the host basalts of these mantle xenoliths have very constant Sr and Nd isotopic compositions.

The isotopic analyses of individual mineral separates and host bulk rocks, and the pyroxenite veins and their wall rocks demonstrate the isotopic disequilibria. Whole rock sample J112C3 has higher $^{87}Sr/^{86}Sr$ and lower $^{143}Nd/^{144}Nd$ ratios than the separated minerals. Two composite xenoliths (H-1 and X-11) have been analyzed for Sr and Nd isotopic ratios for both host lherzolite and pyroxenite veins; in both cases, the veins are higher in radiogenic Nd but lower in radiogenic Sr isotopes than the hosts. In addition, the two veins in H-l lherzolite arc also different in both Sr and Nd isotopic compositions. However, the opposite case has been also found by several authors (Song and Frey, 1989; Tatsumoto et al, 1992). All Nd isotope data from comparative studies on pyroxenite veins and wall rocks for composite xenoliths from Hannuoba are plotted in Fig. 4, which clearly show that the clinopyroxenes of veins and host lherzolites have different Nd isotopic compositions, but the bulk samples of veins and hosts do not show any significant difference.

Table 2 Major element compositions of mantle xenoliths from northern China

Sample	SiO_2	TiO_2	Al_2O_3	Fe_2O_3	FeO	MnO	MgO	CaO	Na_2O	K_2O	P_2O_5	Mg
Kuandian												
C-A	44.90	0.11	2.85	2.17	6.60	0.14	37.81	3.10	0.48	0.03	0.01	88.7
J118C7	47.27	0.15	3.05	1.39	7.28	0.14	36.39	3.46	0.62	0.03	0.02	88.4
J20C18	46.50	0.12	3.50	0.03	6.71	0.15	38.14	3.43	0.98	0.02	0.01	90.9
J36C3	44.62	0.12	3.09	1.83	7.02	0.14	38.09	3.10	0.71	0.03	0.02	88.7
J50C3	43.79	0.10	2.61	2.00	7.06	0.14	42.00	2.51	0.31	0.04	0.02	89.4
J112C3	51.46	0.40	8.31	2.37	4.79	0.14	20.32	11.33	0.75	0.08	0.08	83.9
Huinan												
A-15	46.01	0.08	1.59	0.19	6.33	0.14	40.96	2.50	0.50	0.03	0.01	91.8
A-18	46.92	0.15	2.65	1.92	6.35	0.13	38.20	3.55	0.45	0.04	0.01	89.4
A-20	44.18	0.08	0.89	1.75	7.19	0.13	43.79	0.89	0.33	0.04	0.01	89.9
A-21	48.55	0.26	7.15	2.29	4.26	0.12	26.31	8.90	0.69	0.04	0.01	88.1
A-25	45.13	0.22	2.43	0.63	7.18	0.11	41.42	1.09	0.26	0.10	0.06	90.5
A-26	44.50	0.23	1.75	1.02	6.91	0.13	42.93	0.50	0.20	0.10	0.06	90.7
A-27	46.02	0.11	2.55	2.20	6.60	0.14	38.06	3.33	0.56	0.02	0.01	88.7
Hannuoba												
H-1a	52.82	0.28	4.96	4.42	3.13	0.10	24.46	12.49	0.61	0.02	0.01	86.0
H-1b	49.59	0.21	3.66	0.52	3.18	0.10	23.80	16.66	0.93	0.03	0.01	92.1
H-2	51.72	0.44	3.29	5.78	7.41	0.19	24.24	4.58	0.48	0.04	0.01	77.4
H-3	45.10	0.03	1.52	2.20	6.40	0.13	40.97	1.97	0.66	0.02	0.00	89.7
H-4	48.93	0.14	3.92	2.79	4.17	0.13	33.99	3.70	0.71	0.02	0.00	90.0
X-11	44.66	0.11	3 15	2.38	7.88	0.15	37.20	2.75	0.42	0.02	0.02	86.9
X-11a	48.93	0.28	8.69	2.56	3.84	0.12	24.91	8.98	0.66	0.02	0.02	87.8
X-14	43.30	0.10	2.66	8.83*		0.13	40.90	1.97	0.21	0.01	0.02	90.1

Note: * denotes total iron (data obtained by wet chemistry).

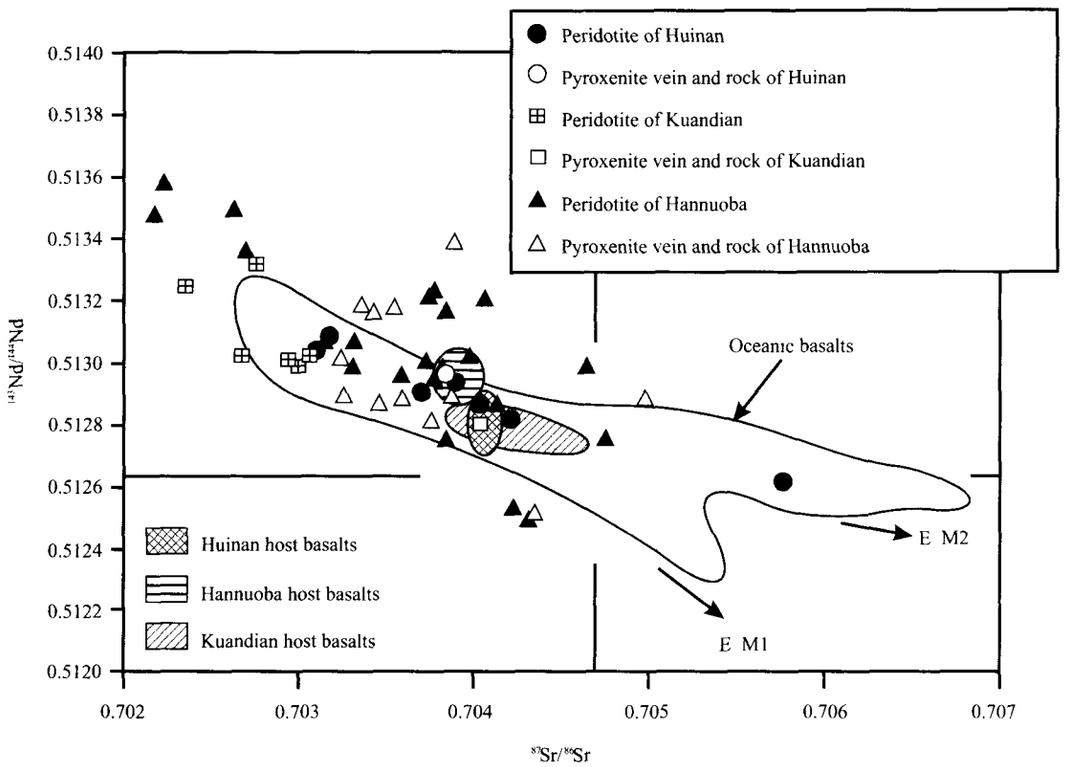

Fig. 3. Sr and Nd isotopic compositions of the mantle xenoliths.
Part of the data for the mantle xenoliths of Hannuoba and Kuandian are from Song and Frey (1989) and Tatsumotoet al. (1992). The data defining the host basalt areas are from Liu et al (1992b) and Song et al. (1990).

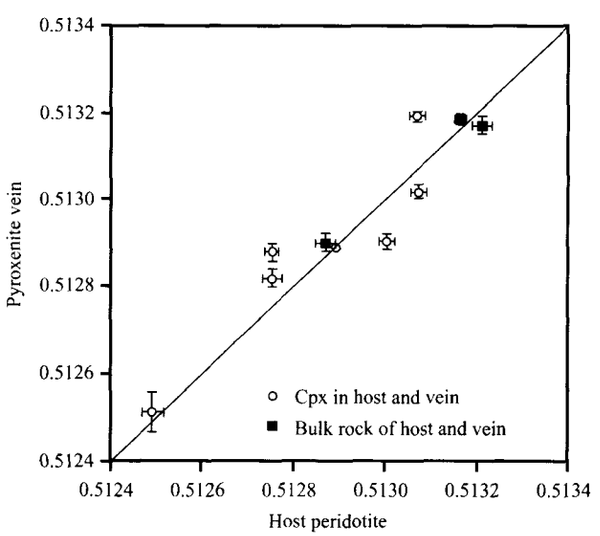

Fig. 4. Comparison of Nd isotopic ratio between pyroxenite veins and their host peridotites from Hannuoba.
Error bars are defined by 2a. Several data are from Tatsumoto et al. (1992) and Song and Frey (1989).

5 Discussion

5.1 Melting processes

Depletion of basaltic components and radiogenic Sr, and enrichment of radiogenic Nd isotopes in the peridotites as compared with the bulk earth are suggestive of origins of the peridotites as residues of partial melting of primitive mantle, although a number of peridotite xenoliths show the LREE enrichment. Based on a world wide survey, McDonough and Frey (1989) found that CaO and Al_2O_3 contents decrease with decreasing HREE abundances in peridotite xenoliths. This is because the HREEs have similar partitioning behavior with the basaltic components, such as Ca and Al, and mantle metasomatism does not significantly disturb the distributions of the HREEs relative to the LREEs. Hence such correlations should be the result mainly of mantle melting.

Unlike the light REEs, which are often decoupled from the major elements, the heavy REE abundances in these xenoliths are correlated with the Al/Si, Ca/Si and Mg/Si ratios (Fig. 5). The Yb abundances are positively

Table 3 Trace element abundances (ppm) and isotopic ratios of bulk rocks and mineral separates of mantle xenoliths from northern China

Sample	La	Ce	Nd	Sm	Eu	Gd	Dy	Er	Yb	Lu	Sr	Ba	Rb	$^{147}Sm/^{144}Nd$	$^{87}Sr/^{86}Sr$	$^{143}Nd/^{144}Nd$
Kuandian																
J118C7cpx	1.80	641	5.17	173	0.666	242	198	1.84	1.66	248	712	nd	nd	0.202	0.702681±17	0.513029±7
J20C18cpx	119	137	2.60	1 12	0.469	1.89	153	1.64	1.52	0.224	41 3	nd	nd	0.161	0.702733±18	0.513321±8
Jl 12C3 cpx	0.997	3.02	185	0.978	0.366	116	1 14	0.472	0 288	0.0367	394	nd	nd	0.208	0.703241±16	0.512901±8
J36C3 cpx	0.540	1.97	2.84	118	0.528	116	169	178	1 63	0.248	35.9	nd	nd	0.273	0.702347±17	0.513248±8
J50C3 cpx	0.552	1.92	111	0.817	0.361	114	1.39	0.862	0.754	0.108	38.5	nd	nd	0.134	0.703063±15	0.51303 1±7
C-A cpx	6.93	15.0	747	1 91	0.697	243	177	173	1.55	0.225	130	nd	nd	0.155	0.702948±16	0.513007±8
C-A uli	0.0628	0.154	0.0717	0.0189	0.00719	0.0273	0.0468	0.0561	0.0865	0.0197	179	nd	nd	0.159	nd	nd
C-A amph	642	118	6.59	171	0.591	106	153	1.63	140	0.111	nd	nd	nd	0.157	0.702971±16	0.512993±8
J112C3 WR	112	478	181	0.884	0.307	1 16	1.34	0.875	0.857	0.133	36.5	nd	nd	0.190	0.704028±12	0.512801±12
Human																
A- 1 5 cpx	1.00	173	131	0.875	0.408	1.63	1 97	1.06	1.08	0.180	32	nd	0.996	0.129	0.703693±18	0.512910±12
A-21 cpx	0.447	177	2.7	1.2	0.52	1.96	154	1.68	1.62	0.148	26.3	1.07	0.0113	0.169	0.703104±19	0.513035±18
A-25 cpx	130	8.30	5.98	1 90	0.743	175	315	2.03	176	156	511	nd	6.67	0 192	0.70388±17	0.512937±9
A-26 cpx	4.30	8.98	4.62	1.11	0.435	148	1 9	119	1 15	0.167	nd	2.2	nd	0.145	0.704022±17	0.512866±9
A-18WR	0.442	1.01	0.705	0.134	0.0913	0.346	0.417	0.271	0.263	0.0399	8.16	5.66	0.952	0 101	0.704205±18	0.512821±9
A-20 WR	0.335	0.761	0.429	0.123	0.0426	0.138	0.123	0.0699	0.061	0.00917	5.40	224	0.266	0 173	0.705749±20	0.512619±9
A-2 1 WR	0.177	0.912	1.32	0.574	0.15	1.02	116	0.852	0.847	nd	113	6.6	0.22	0 163	0.703851±16	0.512972±10
A-27 WR	0.113	0.347	0.347	0.151	0.0648	0.273	0.369	0.236	0.268	nd	3.55	4.16	0.0789	0.263	0.703156±18	0.513084±10
Hannuoba																
H-l cpx	111	172	3.30	1.02	0.373	117	148	0.985	1.03	0.170	48.9	0.501	nd	0 187	0.703827±16	0.512752±12
H-la cpx	1.81	518	4.38	145	0.523	1.86	217	1.34	1 13	0.163	49.5	nd	nd	0.200	0.703741±18	0.512818±10
Il-lbcpx	1.59	4.92	4.48	140	0.496	1.61	176	1.01	0.862	0.126	561	0.373	nd	0 189	0.7034521±17	0.512878±8
PI-2 WR	0.997	193	233	0.67	0.134	0.734	0.629	0.363	0.323	0.0503	nd	3.03	nd	0.174	nd	0.511865±8
H-3 WR	0.428	0.856	0.43	0.0885	0.028	0.0876	0.103	0.085	0.0989	0.0178	nd	0.95	0.143	0.124	0.704752±19	0.512755±10
H-4 WR	0.246	0.605	0.53	0.202	0.0831	0.344	0.488	0.36	0.374	0.0600	7.58	0.502	0.249	0.131	0.703761±17	0.513228±1
X-ll WR	0.085	0.282	0.388	0.8	0.0766	0.317	0.465	0.317	0.317	0.0495	475	0.549	0.667	0.281	0.703831 ±16	0.513 162±8
X-llaWR	0.252	0.786	1.06	0.565	0.237	1.03	145	0.954	0.926	0.142	13	0.804	0.383	0.322	0.703528±18	0.513182±8
X-14 WR	0.197	0.605	0.581	0.233	0.0956	0376	0.499	0.341	0339	0.054	7.56	0.671	nd	0.243	0.703775±16	0.512937±9

Note: errors are 2 σ; cpx – clinopyroxene; oli – olivine; amph – amphibole; WR – whole rock; nd – no data.

correlated with the Al/Si and Ca/Si, and negatively with the Mg/Si. The Yb abundances in clinopyroxenes, however, are not correlated with the major element ratios of their host peridotites, presumably because the Yb distribution in clinopyroxene is not completely controlled by the major element composition of their host peridotites, or that the HREEs in peridotite are not dominantly accommodated in clinopyroxene.

The estimated primitive mantle also falls within the distribution trends of the mantle xenoliths in the figure, which is suggestive of formation of these mantle xenoliths by different degrees of magma extraction from the primitive mantle. Therefore, the variations in major element ratios and the Yb abundances can be used to estimate the degrees of magma extraction of the mantle according to mass balance. However, it is difficult to quantify the degree of partial melting of the mantle because of the difficulties to choose the chemical compositions of the extracted magma and primitive mantle. It can be summarized that the variations of basaltic components and HREEs in the peridotite xenoliths do suggest that the mantle had undergone various degrees of partial melting.

5.2 Melt/fluid metasomatism

5.2.1 Origin of the diverse REE patterns

The REE patterns observed for the clinopyroxene separates and whole-rock peridotites are diverse: many REE patterns of whole-rock peridotites and their clinopyroxene separates are LREE-enriched, among which some are U-shaped and some show "spoon-shaped" LREE patterns. One lherzolite from the Kuandian area contains amphibole, and clinopyroxene and amphibole separates from this xenolith show considerably LREE-enriched patterns (Fig. 2b). These types of REE patterns must have been derived from enrichment processes affecting large ion lithosphile elements due to magma/fluid metasomatism.

A chromatographic-type melt migration process acting on a LREE-depleted mantle composition is most likely responsible for the origin of the variable LREE-enrichment, especially the U-shaped REE patterns (e.g. Navon and Stolper, 1987; Bodinier et al., 1990; Kelemen et al., 1990; Hauri and Hart, 1994). In this model, the degrees of LREE-enrichment, or variations in shape of REE patterns depend on the time for the melt to pass through the mantle column or on the distance from the input point of the melt. However, judging from the covariations between the Yb abundances and the major element contents, it may be that these peridotites were formed as the residues of magma extraction of different degrees. Therefore, the REE compositions of these peridotites are better interpreted as the products both of partial melting of variable percentages and mixing with different amounts of a small-volume melt strongly enriched in incompatible elements. This model has been employed by many authors (e.g. Frey and Green, 1974; Song and Frey, 1989) to account for the enrichment of incompatible elements in depleted mantle rocks.

The harzburgite H-3 has a U-shaped REE pattern, a relatively high MgO content, and low Al_2O_3, CaO and HREE contents, while the spinel lherzolite H-4 has the lowest MgO and highest CaO and Al_2O_3 contents among these peridotite xenoliths. This striking contrast in the chemical composition for these two peridotites shows that they experienced remarkably different degrees of melt extraction. A model calculation carried out to constrain the

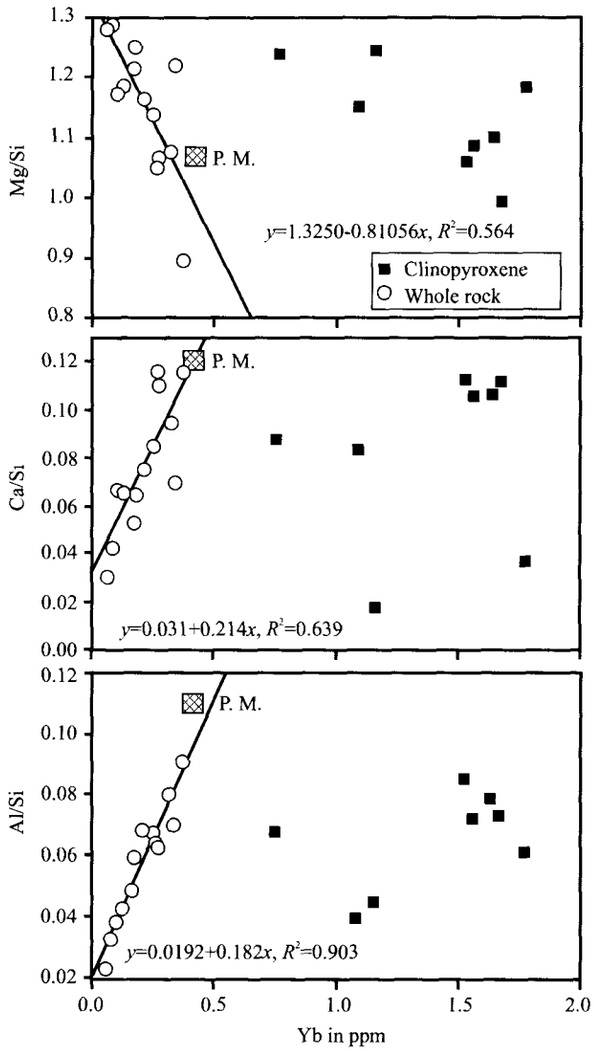

Fig. 5. Major element versus Yb plot for the mantle xenoliths from north China.
The major element data of the primitive mantle are from McDonough (1990), and the Yb content of the primitive mantle from Hofmann (1988).

origins of the REE patterns of these two peridotites shows that the U-shaped REE pattern of the harzburgite H-3 and the spoon-shaped REE pattern of the spinel lherzolite H-4 are well modeled through mixing 1% mass of melt with the depleted mantle residues formed by 15% and 6% fractional melting respectively of the primitive mantle (Liu et al., 1996). The REE compositions of the peridotites depend on the melting degree and mineralogy of the initial source and residues. A simple LREE-enriched pattern without U-shape and spoon-shape could be produced by mixing a relatively large amount of melt with residual mantle.

5.2.2 REE geochemistry of vein-host interaction

The REE patterns of clinopyroxenes from two veins in the lherzolite H-1 are generally similar, but have differences in HREE contents (Fig. 2d). This indicates that the magmas in equilibrium with these two veins probably had different REE compositions, though these two veins formed just 10 cm apart. The clinopyroxene separates from the host xenolith have a REE pattern similar to those of the two veins, but with a progressive increase from Dy to Lu. This is similar to the observations of Bodinieret al. (1990) for the host harzburgite at < 15 cm from the contact of a 65cm harzburgite section perpendicular to an amphibole pyroxenite vein from the Lherz massif. These patterns have been interpreted by the authors (Bodinier et al., 1990) as being due to the diffusion-controlled metasomatism by a silicate melt. The REE patterns of the bulk-rock vein and host for the composite xenolith X-11 are not distinguishable. These observations indicate that the pyroxenite veins and host lherzolites at <10 cm from the vein-host border can approach to chemical equilibrium.

As discussed above, the pyroxenite xenoliths and veins have two types of REE patterns, and hence the melts from which they were crystallized might be different. Assuming that these pyroxenite xenoliths and veins were once equilibrated with their parent magmas, the REE compositions of their parent magmas can be calculated based on mineral/melt bulk partition coefficients. The calculated REE patterns indicate that their parent magmas were not their host alkalic basalts and also not the tholeiitic basalts in the Hannuoba volcano (Liu et al. 1996). The calculated REE compositions are characterized by significantly high HREE contents, as compared with the erupted basalt magmas, and might have originated from large-degree partial melting of spinel-stable peridotite mantle. Moreover, the magmas equilibrated with the pyroxenites with convex-upward REE patterns show high LREE-enrichment as compared with those equilibrated with the pyroxenites which have LREE-depleted patterns.

5.2.3 Metasomatic agent(s)

Two main types of metasomatizing agents are generally invoked in most interpretations of the metasomatized mantle peridotites; silicate melt and H_2O- or CO_2-rich, or H_2O-NaCl fluid (e.g. Frey and Green, 1974; Gurney and Harte, 1980; Stosch and Seek, 1980; Menzies and Murthy, 1980; Boettcher and O'Neil, 1980; McDonough and McCulloch, 1987; O'Reillyand Griffin, 1987; Brenan, 1993; Coltorti et al., 1999). On the basis of the geochemical characteristics of the SE China clinopyroxenes, Xu et al. (2003) suggested that the mantle beneath SE China has undergone metasomatism either by sequential events with different compositions (one silicate and one carbonatitic) or by a single event with a complex silicate fluid rich in both H_2O and CO_2 components. Aspects of the chemical interactions of both types of the metasomatizing agents with the mantle country rocks through which they traverse can be described by a chromatographic column model (Navon and Stolper, 1987). The peridotites with modified chemistry veined by pyroxenites provide at least some direct evidence that metasomatism was dominated by magmatic processes. Basaltic melts migrating through mantle matrix will make their country rocks enrichment in basaltic components and HREEs and depletion in Mg and Ni, and infiltration of the melts from conduits into the host refractory peridotites can result in both cryptic and modal metasomatism (Bodinier et al., 1990). Therefore, in the case of the mantle xenoliths studied here, the silicate melt(s) from which the pyroxenites were precipitated most likely metasomatized the mantle. However, volatile-rich fluid must have played a key role in the metasomatic processes, because the chemistry of metasomatism is better interpreted in terms of crystal/fluid partitioning, as discussed in the following.

Sr/Ba and La/Ba ratios in the peridotites and pyroxenites vary over three orders of magnitude (Fig. 6). The clinopyroxene separates from peridotites, pyroxenite xenoliths and veins generally have high Sr/Ba and La/Ba ratios relative to the whole rocks, because of the different cpx/melt and bulk-rock/melt partition coefficients for these elements. Nevertheless, the data for both clinopyroxene separates and whole rocks show a similar distribution trend. One may suspect the data array to be the result of different degrees of magma extraction since the Sr/Ba and La/Ba could be significantly fractionated during melting processes. However, both ratios do not show systematic change with variation of elemental abundances in these xenoliths, and this argues against a partial melting process. Consequently, the data distribution in the figure is better interpreted in terms of mixing between two components due to mantle metasomatism. The end of the data array with high Sr/Ba and La/Ba ratios reflects the depleted mantle, and the model depleted mantle plots close to this end. The

other end has element ratios even lower than those of the Cenozoic basalts in eastern China, so the possibility that basaltic magmas played the part of the metasomatic agent can be ruled out. Mixing with a component with much lower Sr/Ba and La/Ba ratios is needed to create the observed mixing trend.

From the correlation shown in Fig. 6 and the LREE-enriched REE patterns shown in Fig. 2, the metasomatism agent should have had a signature of high LREE/HREE, and low La/Ba and Sr/Ba ratios. Such low element ratios have been often found in phlogopite-bearing xenoliths, e.g. the phlogopite peridotites from Kimberley of South Africa and the phlogopite clinopyroxenite nodules from the Roccamonfina Volcano of Italy. The formation of these phlogopite xenoliths, regardless of their shallow (crust) level (Giannetti and Luhr, 1990) or deep (mantle) level origin (Hawkesworth et al., 1990), must have been related to a volatile-rich fluid. Such an alkali-chloride-rich aqueous fluid not only has high fluid/mineral and fluid/melt partition coefficients but also shows a strong fractionation of some trace elements, and is considered to play an important role in forming calc-alkaline arc magmas by melting of the mantle wedge above the subducted slab and transporting trace elements in the subduction zone (e.g. Tatsumi et al., 1986; McCulloch and Gamble, 1991; Davies and Stevenson, 1992; Ayers et al., 1995; Keppler, 1996). The fluid calculated to be in equilibrium with the mantle peridotite has ratios low enough to account for the lowest ratios in the xenoliths, as shown in Fig. 6. The candidate for the metasomatic agent that could produce the extremely low Sr/Ba and La/Ba ratios in the enriched mantle may be the fluids generated in an ancient subduction zone due to the dehydration of subducted slab, or a volatile-rich silicate melt formed by fluid-triggered melting in the mantle wedge above the subducted slab, or formed by low-degree melting in the lower portion of the mantle. In any case, the involvement of fluid extremely enriched in Ba over Sr and La in the mantle metasomatism is needed to explain the geochemical signatures of the enriched mantle.

5.3 Timing of mantle processes

The information recorded in the model ages of these xenoliths suggests multiple events in the evolution history of the mantle. In Fig. 7, we have plotted the data for samples from the three volcanoes into Sm-Nd isochron diagram. Positive correlations between $^{147}Sm/^{144}Nd$ and $^{143}Nd/^{144}Nd$ are observed for these three suites of mantle xenoliths, which suggest a long-term effect of mantle processes on the isotopic composition of the mantle.

The data on Hannuoba xenoliths, combined with those previously published by several authors, permit a detailed analysis of the timing of the mantle processes. The majority of the data tend to fall on or close to a straight line, the slope of which corresponds to an age of 335 Ma. One phlogopite pyroxenite studied by Tatsumoto et al. (1992) and one pyroxenite studied in this work have remarkably low $^{147}Sm/^{144}Nd$ and $^{143}Nd/^{144}Nd$ ratios, indicating old ages for melting events. One of these two xenoliths has a model age of about 2.7 Ga, but the other has a model T_{CHUR} age older than the earth. Combined with the primitive and depleted mantle, these two pyroxenite and several peridotite xenoliths fall along a straight line with 2.7 Ga reference age. The data distributions of xenoliths from the Huinan and Kuandian areas in the figure may be best depicted by two reference isochrons. These isochrons yield reference ages respectively of about 0.6–1.0 Ga and 280–400 Ma. The ages of "isochrons" shown in the figure are suspectable, because original isotopic signatures of the mantle are subject to modification by later geochemical processes. However, the positive relationships between Sm/Nd and Nd isotope ratios suggest that at least two or more mantle events took place a relatively long time ago and are responsible for the isotopic composition of the mantle. Since the isotopic compositions are decoupled from the major and

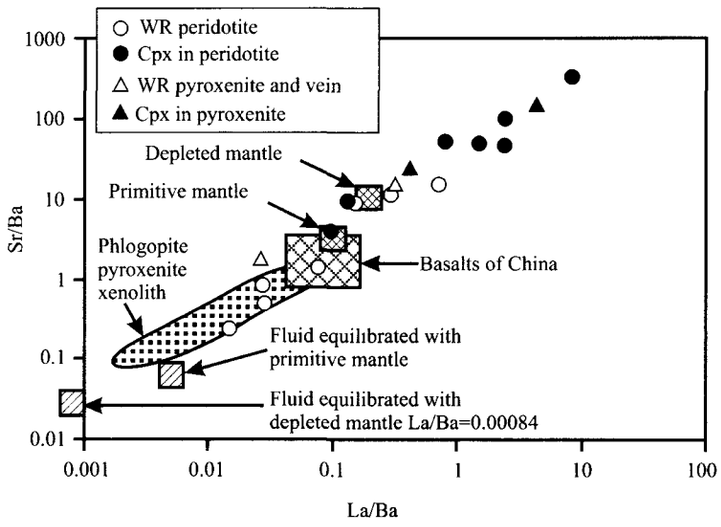

Fig. 6. Sr/Ba versus La/Ba variation of the mantle xenoliths from north China. Data sources: depleted and primitive mantle from Hofmann (1988); basalts of China from Liu et al. (1994); phlogopite pyroxenite xenoliths from Giannetti and Luhr (1990). The fluids equilibrated with the primitive and depleted mantle were calculated as fluid/rock partition coefficients ($D^{fluid/rock}$), which were obtained from the equation $D^{fluid/rock}=D^{fluid/melt}/D^{rock/melt}$. The fluid/melt partition coefficients ($D^{fluid/melt}$) were from Keppler (1996), and the rock/melt partition coefficients ($D^{rock/melt}$) were calculated from the mineral/melt partition coefficients based on the assumed mineral compositions for the depleted and primitive mantle. The mineral/melt partition coefficients compiled by Bedard (1994) for these elements were used in the calculation of $D^{rock/melt}$.

trace element compositions, the inferred relatively young events from the $^{147}Sm/^{144}Nd$ versus $^{143}Nd/^{144}Nd$ correlations suggest metasomatism rather than melting processes for these mantle rocks.

Recently, there is increasing interest in studying the relationships among mantle events recorded by mantle xenoliths and the associated crustal orogeny and tectonics (e.g. Hawkesworth etal., 1990; Beard and Glazner, 1995). We can not say much about the true significance of the inferred ages for mantle processes, but we think they may be tested by the record of the mantle events kept in the crustal materials, since the overlying crust should have had response to the mantle processes. The first stage in the formation of the continental nuclei of the Sino-Korean Craton is conventionally considered to end with the Fupingian Orogeny at about 2.5–2.6 Ga ago (Yang et al., 1986; Zhang et al., 1986). The mantle events of 0.6–1.0 Ga are possibly correlated with main tectonic and magmatic episodes (Jinningian and Sibaoan episodes) of the Jinningian. Xu et al. (2003) estimated an age of about 733 Ma based on the Sm/Nd versus $^{143}Nd/^{144}Nd$ correlations of the Nushan clinopyroxene SE China, and considered it as a minimum age for the major element depletion event in the mantle. The mantle processes that took place 200–400 Ma ago might be accompanied by the convergence of the Yangtse and Sino-Korean Craton to create Palasia. Although the age estimates for the mantle events have large uncertainty, these episodes recorded in the Sm-Nd isotope system for the mantle samples could be related to the main events recorded in the basement rocks of the Sino-Korean Craton and its adjacent orogenic belts. However, studies are still needed to understand the true meanings of the estimated ages.

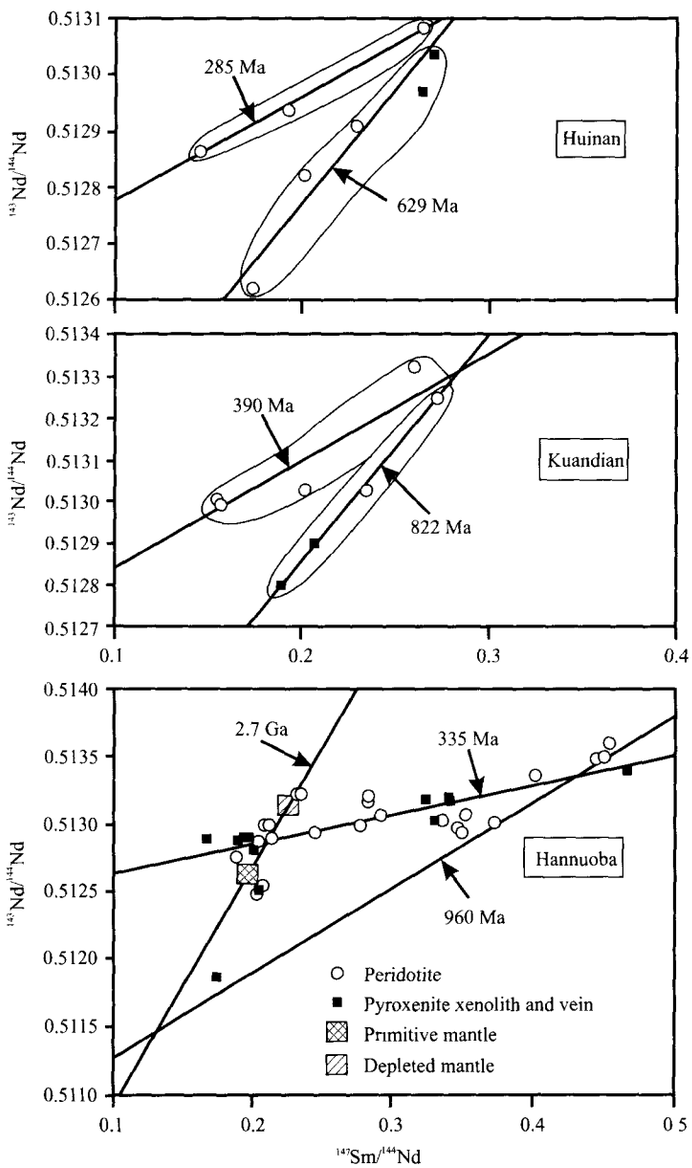

Fig. 7. Sm/Nd versus Nd isotope ratio diagrams for these three suites of mantle xenoliths from north China.

6 Conclusions

The major part of the lithospheric mantle beneath the Chinese continent is chemically and isotopically very heterogeneous, showing complex incompatible element-enriched and depleted features. The diversity of REE geochemistry for the mantle xenoliths can be ascribed to mantle metasomatism superimposed on fractional melting of variable percentages. The mantle metasomatic agent was enriched in Ba over Sr and La, and may have been a volatile-rich silicate melt possibly derived from the fluid-induced melting in an ancient subduction zone.

The highly variable isotopic compositions and their decoupling from trace element compositions strongly indicate a complex evolution history of the mantle. The mantle may have been first depleted from the CHUR source at an early age, and the most depleted mantle peridotite may have resulted from multiple depletion events. The correlations between Sm/Nd and Nd isotopic ratios in these mantle xenoliths suggest at least two main mantle events most likely responsible for the enrichment of large ion lithosphile elements in the mantle.

Acknowledgement

This research was partly supported by the Chinese Academy of Sciences under the Innovation Project KZCX3-SW-124.

Manuscript received June 15, 2004
accepted Aug. 15, 2004
edited by Liu Xinzhu

References

Ayers, J.C., and Eggler, D.H., 1995. Partitioning of elements between silicate melt and FEO-NaCl fluids at 1.5 and 2.0 Gpa pressure: Implications for mantle metasomatism. *Geochim. Cosmochim. Acta*, 59: 4237–4246.

Basu, A.R., Wang, J., Huang, W., Xie, G., and Tatsumoto, M., 1991. Major element, REE, and Pb and Sr isotopic geochemistry of Cenozoic volcanic rocks of eastern China: implications for their origin from suboceanic-type mantle reservoirs. *Earth Planet. Sci. Eett.*, 105: 149–169.

Beard, B.E., and Glazner, A.F., 1995. Trace element and Sr and Nd isotopic composition of mantle xenoliths from the Big Pine volcanic field, California. *J. Geophys. Res.*, 100: 4169–4179.

Bedard, J.H., 1994. A procedure of calculating the equilibrium distribution of trace elements among the minerals of cumulate rocks, and the concentration of trace elements in the coexisting liquids. *Chem. Geol.*, 118: 143–153.

Bodinier, J.E., Vasseur, G., Vernieres, J., Dupuy, C., and Fabrics, J., 1990. Mechanisms of mantle metasomatism: Geochemical evidence from the Eherz erogenic peridotite. *J. Petrol.*, 31: 597–628.

Boettcher, A. E., and O'Neil, J.R., 1980. Stable isotope, chemical, and petrographic studies of high pressure and amphiboles and micas: Evidence for metasomatism in the mantle source regions of alkali basalts and kimberlites. *Am. J. Sci.*, 280A: 594–621.

Brenan, J.M., 1993. Partitioning of luorine and chlorine between apatite and aqueous fluids at high pressure and temperature: implications for the F and Cl content of high P-T fluids. *Earth Planet. Sci. Eett.*, 117: 251–263.

Coltorti, M., Bonadiman, C., Hinton, R.W., Siena, F., and Upton, B.G.J., 1999. Carbonatite metasomatism of the oceanic upper mantle: evidence from clinopyroxenes and glasses in ultramafic xenoliths of Grande Comore, Indian Ocean. *J. Petrol.*, 40: 133–165.

Cong, B., and Zhang, R., 1983. Petrogenesis of Hannuoba basalts and their ultramafic inclusions (in Chinese). *Scientia Sinica*, 26: 308–315.

Davies, J.H., and Stevenson, D.J., 1992. Physical model of source region of subduction zone volcanics. *J. Geophys. Res.*, 97: 2037–2070.

Frey, F.A., and Green, D.H., 1974. The mineralogy geochemistry and origin of Iherzolite inclusions in Victorian basanites. *Geochim. Cosmochim. Acta*, 38: 1023–1050.

Giannetti, B., and Luhr, J.F., 1990. Phlogopite-clinopyroxenite nodules from high-K magmas, Roccamonfina Volcano, Italy: evidence for a low-pressure metasomatic origin. *Earth Planet. Sci. Lett.*, 101: 404–424.

Gurney, J. and Harte, B., 1980. Chemical variations in upper mantle nodules from Southern African kimberlites. *Phil. Trans. R. Soc. Lond.*, 297, 273–293.

Harte B., 1983. Mantle peridotites and processes-the kimberlite sample. In: Hawkesworth, C.J., and Norry, M.J. (eds.), *Continental Basalts and Mantle Xenoliths*, Shiva: Nantwich, Cheshire, 46–91.

Hauri, E.H., and Hart, S.R., 1994. Constraints on melt migration from mantle plumes: A trace element study of peridotite xenoliths from Savai'i, Western Samoa. *J. Geophys. Res.*, 99: 24301–24321.

Hawkesworth, C.J., Erlank, A.J., Kempton, P.D., and Waters, F. G., 1990. Mantle metasomatism: Isotope and trace-element trends in xenoliths from Kimberley, South Africa. *Chem. Geol.*, 85: 19–34.

Ho, K., Chen, J., Smith, A.D., and Juang, W., 2000. Petrogenesis of two groups of pyroxenite from Tungchihsu, Penghu Island, Taiwan Strait: implications for mantle metasomatism beneath SE China. *Chem. Geol.*, 167: 355–372.

Hofmann, A.W., 1988. Chemical differentiation of the Earth: the relationship between mantle, continental crust, and oceanic crust. *Earth Planet. Sci. Lett.*, 90: 297–314.

Johnson, K.T.M., Dick, H.J.B., and Shimizu, N., 1990. Melting in the oceanic upper mantle: an ion microprobe study of diopside in abyssal peridotites. *J. Geophys. Res.*, 95: 2661–2678.

Kelemen, P.B., Johnson, K.T.M., Kinzler, R.J., and Irving, A.J., 1990. High field strength element depletions in arc basalts due to mantle-magma interaction. *Nature*, 345: 521–524.

Keppler, H., 1996. Constraints from partitioning experiments on the composition of subduction-zone fluids. *Nature*, 380: 237–240.

Liu, C.-Q., Masuda. A., Shimizu, H., Takahashi, K., and Xie, G-H., 1992a. Evidence for pressure dependence of the peak position in the REE mineral/melt partition patterns of clinopyroxene. *Geochim. Cosmochim.* Acta, 56: 1523–1530.

Liu, C.-Q., Masuda, A. and Xie, G-H., 1992b. Isotope and trace element geochemistry of alkali basalts and associated megacrysts from the Huangyishan volcano, Kuandian, Liaoning, *China. Chem. Geol.*, 97: 219–231.

Liu, C.-Q., Masuda. A., and Xie G-H., 1994. Major- and trace-element compositions of Cenozoic basalts in eastern China: Petrogenesis and mantle source. *Chem. Geol.*, 114: 19–42.

Liu, Chongqiang, Xie Guanghong and Masuda, A., 1996. REE and Sr and Nd isotope geochemistry of mantle xenoliths from basalts in Hannuoba. *Acta Petrologica Sinica*, 12: 382–389 (in Chinese with English abstract).

Lu Fengxiang., Molan, E., and Deng Jingfu, 1983. Ultramafic inclusions and megacrysts in alkaline basalts from Huangyishan, Kuandian, Liaoning Province, China. *Petrological Research*, No.3: 77–88 (in Chinese).

Luo Zhaohua, 1984. Ultramafic inclusions in Dayishan basalts, Huinan, Jiling Province, China. *Earth Science* 1: 73–80 (in Chinese).

McCulloch, M.T., and Gamble, J.A., 1991. Geochemical and geodynamical constraints on subduction zone magmatism. *Earth. Planet. Sci. Lett.*, 102: 358–374.

Menzies, M.A., and Murthy, V.R., 1980. Mantle metasomatism as a precursor to the genesis of alkaline magmas: Isotopic evidence. *Am. J. Sci.*, 280A: 622–638.

McDonough, W.F., and Frey, F.A., 1989. REE in upper mantle

rocks. In Geochemistry and Mineralogy of Rare Earth Elements. In: Lipin, B., and McKay, G.R. (eds.), *Mineral.* Soc. Am., Chelsea, Mich. 99–145.

McDonough, W.F., 1990. Constraints on the composition of the continental lithospheric mantle. *Earth Planet. Sci. Lett.*, 101: 1–18.

McDonough, W.F. and McCulloch, M.T., 1987. The Southeast Australia lithospheric mantle: Isotopic and geochemical constraints on its growth and evolution. *Earth Planet. Sci. Lett.*, 86: 327–340.

Navon, O., and Stolper, E., 1987. Geochemical consequences of melt percolation: The upper mantle as a chromatographic column. *J. Geol.*, 95: 285–307.

O'Reilly, S.Y., and Griffin, W.L., 1987. Mantle metasomatism beneath western Victoria, Australia: I. Metasomatic processes in Cr-diopside lherzolites. *Geochim. Cosmochim. Acta,* 52: 433–447.

Song, Y., and Frey, F.A., 1989. Geochemistry of peridotite xenoliths in basalt from Hannuoba, Eastern China: Implications for subcontinental mantle heterogeneity. *Geochim. Cosmochim. Acta.* 53: 97–113.

Song, Y., Frey, F.A., and Zhi, X., 1990. Isotopic characteristics of Hannuoba basalts. Eastern China: Implications for their petrogenesis and the composition of subcontinental mantle. *Chem. Geol.*, 85: 35–52.

Stosch, H.G., and Lugmair, G.W., 1986. Trace element and Sr and Nd isotope geochemistry of peridotite xenoliths from the Eifel (West Germany) and their bearing on the evolution of the subcontinental lithosphere. *Earth Planet. Sci. Lett.*, 80: 281–298.

Stosch, H.G., Lugmair, G.W., and Kovalenko, V.I., 1986. Spinel peridotite xenoliths from the Tariat Depression, Mongolia. II: Geochemistry and Nd and Sr isotopic composition and their implications for the evolution of the subcontinental lithosphere. *Geochim. Cosmochim. Acta,* 50: 2601–2614.

Stosch, H.G. and Seek, H.A., 1980. Geochemistry and mineralogy of two spinel peridotite suites from Dreiser Weiher, West Germany. *Geochim. Cosmochim. Acta*, 44: 457–470.

Tatsumi, Y., Hamilton, D.L., and Nesbitt, R.W., 1986. Chemical characteristics of the fluid phase released from a subducted lithosphere and the origin of arc magmas: evidence from high pressure experiments and natural rocks. *J. Volcanol. Geotherm. Res.*, 29: 293–309.

Tatsumoto, M., Basu, A.R., Huang, W., Wang, J., and Xie, G., 1992. Sr, Nd, and Nd isotopes of ultramafic xenoliths in volcanic rocks of Eastern China: enriched components EMI and EMU in subcontinental lithosphere. *Earth Planet. Sci. Lett.*, 113: 107–128.

Tatsumoto, M., and Nakamura, Y., 1991. DUPAL anomaly in the Sea of Japan: Pb, Nd, and Sr isotopic variations at the eastern Eurasian continental margin. *Geochim. Cosmochim. Acta,* 55: 3697–3708.

Tu, K., Rower, M.F.J., Xie, G., Carlson, R.W., Wang, Q., and Zhang, M., 1989. Lead isotopic data for Cenozoic basalts from eastern China: evidence for cratonic and circum-cratonic mantle domains. *Abstr. 28th Int. Geol. Congr. Washinton, D.C.*, 3: 260–261.

Xu, X., O'Reilly, S. Y., Griffin, W.L., and Zhou, X., 2003. Enrichment of upper mantle peridotite: petrological, trace element and isotopic evidence in xenoliths from SE China. *Chem. Geol.*, 198: 163–188.

Yang, Z., Cheng, Y., and Wang, H., 1986. *The Geology of China.* Oxford: Clarendon Press.

Zhang, W., Li, Y., Ma, F., and Zhang, C., 1986. The marine and continental geotectonic cycles and evolution of China and its environs. In: Zhang Wenyu (ed.), *Marine and Continental Geotectonics of China and its Evrirons.* Beijing: Academic Press, 22–44 (in Chinese).

Zhang, M., Suddaby, P., O'Reilly, S.Y., Norman, M., and Qiu, J., 2000. Nautre of the lithospheric mantle beneath the eastern part of the Central Asian fold belt: mantle xenolith evidence. *Tectonophysics*, 328: 131–156.

Zheng, J., 1998. Nature and evolution of Cenozoic lithospheric mantle beneath Shandong Penisula, Sino-Korean Craton, Eastern China. *Intl. Geol. Rev.*, 40: 471–499.

Zheng, J., O'Reilly, S.Y., Griffin, W.L., Lu, F., Zhang, M., and Pearson, N.J., 2001. Relict refractory mantle beneath the eastern North China block: significance for lithosphere evolution. *Lithos*, 57: 43–66.